Available online at www.sciencedirect.com
SCIENCE DIRECT
Journal of Nuclear Materials 349 (2006) 182–194
journal of nuclear materials
www.elsevier.com/locate/jnucmat

Experimental study on the oxidation of nuclear graphite and development of an oxidation model

Eung Soo Kim *, Hee Cheon NO

Department of Nuclear and Quantum Engineering, Korea Advanced Institute of Science and Technology, 373-1, Guseong-dong, Yuseong-gu, Daejeon 305-701, Republic of Korea

Received 9 August 2005; accepted 26 October 2005

Abstract

The present study investigates the graphite oxidation, which is one of the most serious problems during an air-ingress accident of a high temperature gas-cooled reactor (HTGR). In our study, oxidation experiments have been performed for IG-110 graphite by gas analysis under the various temperatures and oxygen concentrations. As a result, the order of reaction (n) and activation energy (E_a) were estimated as 0.75 ± 0.146 and 218 ± 3.76 kJ/mol, respectively within a 95% confidence level. The CO/CO_2 ratios were also measured and compared with Aurthur's and Rossberg's correlations. Most of data lie between their predictions, but for better prediction, an empirical correlation was newly developed. We measured reaction rates and analyzed them with a computational fluid dynamics (CFD) simulation by incorporating the oxidation parameters and the CO/CO_2 ratio estimated here. Finally, an analytical model that includes both the chemical reaction and mass transfer was proposed and validated against experimental data.

1. Introduction

High temperature gas-cooled reactors (HTGR), due to their passive safety features and usefulness for high heat application including hydrogen production, are anticipated to represent the next generation nuclear reactor. At present, the most critical event expected in this type of reactor is an air-ingress accident, which is caused by a pipe break. When air is ingressed into the reactor due to an accident, the graphite materials in the moderator and reflector suffer from a chemical reaction with oxygen. Such a situation would have serious consequences causing temperature increase by heat generation, damage of structural integrity and accumulation of explosive CO gas in the reactor.

There are numerous reactions of concern among them, they are as follows [1]:

$$C + aO_2 \rightarrow bCO + cCO_2 : \text{ Graphite oxidation reaction} \quad (1)$$

$$C + CO_2 \leftrightarrow 2CO : \text{ Boudouard reaction} \quad (2)$$

$$2CO + O_2 \leftrightarrow 2CO_2 : \text{ CO combustion reaction} \quad (3)$$

* Corresponding author. Tel.: +82 42 869 3857; fax: +82 42 869 3895.
E-mail address: kes@nsys.kaist.ac.kr (E.S. Kim).

0022-3115/$ - see front matter © 2005 Elsevier B.V. All rights reserved.
doi:10.1016/j.jnucmat.2005.10.015

Nomenclature

A	apparent surface area (m^2)
B_m	blowing factor
C_{b,O_2}	bulk oxygen concentration (mol/m^3)
C_{s,O_2}	interfacial oxygen concentration (mol/m^3)
C_p	heat capacity (J/kg K)
d	effective diameter (m)
D	diffusion coefficient (m^2/s)
D_{ij}	binary diffusion coefficient of species i and j (m^2/s)
$D_{O_2,m}$	effective diffusion coefficient of oxygen (m^2/s)
E_a	activation energy (kJ/mol)
f_{CO/CO_2}	CO/CO_2 ratio
h	specific enthalpy (J/kg)
J_i	diffusion flux of species i (kg/m^2 s)
k	reaction rate constant (kg/m^2 s Pa^n)
K_0	pre-exponent factor (kg/m^2 s Pa^n)
k_{cond}	thermal conductivity (W/m K)
k_m	mass transfer coefficient (m/s)
K_m	$K_m = M_c \cdot (2f_{CO/CO_2} + 1)/(f_{CO/CO_2} + 1) \cdot k_m$ (kg m/mol s)
$M_{w,i}$	molecular mass of species i (kg/mol)
m''	mass flux (kg/m^2 s)
$\dot{m}_i$	mole flow rate of species i (mole/s)
n	order of reaction
p	static pressure (Pa)
P_{O_2}	oxygen pressure at reacting surface (Pa)
$P_{O_2,b}$	oxygen pressure in bulk flow (Pa)
r_g	graphite oxidation flux (kg/m^2 s)
r_i'''	generation rate of species i (kg/m^3 s)
r_{cb}	asymptotic chemical reaction flux (kg/m^2 s)
r_{mb}	asymptotic mass transfer flux (kg/m^2 s)
R	gas constant
R_g	graphite oxidation rate (kg/s)
R_{cb}	asymptotic chemical reaction rate (kg/s)
R_{mb}	asymptotic mass transfer rate (kg/s)
Re	Reynolds number
Sc	Schmidt number
Sh	Sherwood number
S_m	mass generation rate (kg/m^3 s)
S_{heat}	heat generation rate (J/m^3 s)
t	time (s)
T	temperature (K)
v	velocity (m/s)
X_i	mole fraction of species i
Y_i	mass fraction of species i
ρ	density (kg/m^3)
μ	viscosity (kg/m s)

In order to investigate the effects, we need a good prediction of the oxidation rate and the CO/CO_2 ratio for various conditions. Reaction (1) can be divided into 3 regimes, depending on the oxidation temperature [1]. At low temperature, the reaction velocity is limited by the chemical reaction rate, since oxygen can penetrate the whole porous graphite with a small concentration gradient (Zone 1). At high temperature (Zone 3), the reaction velocity is determined only by the mass transfer rate to the graphite surface. At intermediate temperatures (Zone 2), the reaction velocity is affected by both chemical and mass transfer rates. The transition temperature of each regime is known to depend on the kinetic parameters and the mass transfer coefficient.

Generally, the chemical reaction rate is related to the material characteristics and the mass transfer rate is associated with gas flow characteristics. Until recently, since many researchers have been investigated the chemical characteristics of graphite oxidation, in the present study we have focused on the prediction of reaction rates covering the whole regime from Zone 1 to Zone 3. First, we measured the oxidation parameters for various conditions and estimated them by comparison with the previous results. Then we incorporated these parameters into a computational fluid dynamics (CFD) code. We subsequently compared the calculations to the experimental data. Finally, we developed and validated a correlation applicable for a system analysis tool.

2. Experiments

The experimental work was divided into the following two parts: (a) pretest (measurement of oxidation parameters) (b) main test (measurement of oxidation rate and gas components under accident conditions).

The pretest was carried out in Zone 1, where mass transfer effects are negligible. This was confirmed by several pretests at different flow rates. In this experiment, the two main oxidation parameters, activation energy (E_a) and order of reaction (n) were

measured. We conducted 15–20 tests for one specimen based on the results of Fuller and Okoh [3] that the activation energy is not affected by the degree of burn-off. And we also did not see any dependency on the kinetic parameters by the burn-off degree though the maximum burn-off was only within 5% in our study. As the number of experimental set increased, the degree of burn-off also increased. And this increase of burn-off raised the reaction rate in a long period of time. This increase of reaction rate made us easily detect the emitted gases, and reduced the experimental error. Since the main focus of the pretest was not on the rate of reaction but on the kinetic parameters, this approach was reasonable.

In the other hand, since the focus of the main test was on the rate of reaction, every data was obtained for different specimens in the induction period. The main test was performed between 700 and 1500 °C to determine the overall reaction rate and the CO/CO_2 ratio at similar conditions to those of an accident.

2.1. Apparatus and experimental conditions

We obtained the oxidation rates by using gas concentration data (see Fig. 1). This method offers two advantages: (1) faster and more precise response than a general thermogravimetric analysis (TGA) and (2) availability of direct analysis for gases such as CO and CO_2. A He/O_2 mixture gas was injected into the test section with a concentration that is controlled by a mass flow controller (Brooks), and a graphite sample was heated by a 15 kW induction heater. The reaction rate was calculated by a gas components analysis through two non-dispersive infrared (NDIR) analyzers (Rosemount NGA2000, Yokogawa IR100).

The test section was made of a cylindrical quartz tube. In order to maintain a hydraulically fully developed flow, a long entry length was designed. This gave us a well-known flow field (Hagen–Poiseuille flow) around the surface of the test specimen. The specimen was installed at the center of the test section and a ceramic rod supported it. The diameter and height of the specimen were 2.1 cm and 3 cm and the diameter of the test-section was 7.6 cm. An induction heater was used for heating the sample and its temperature was measured by a non-contact technique using two infrared thermometers (IRtex Raymatic 10, Raytec Ranger 3i). Setting temperature could be achieved within 30 s by the induction heating method without disturbing the gas flow field.

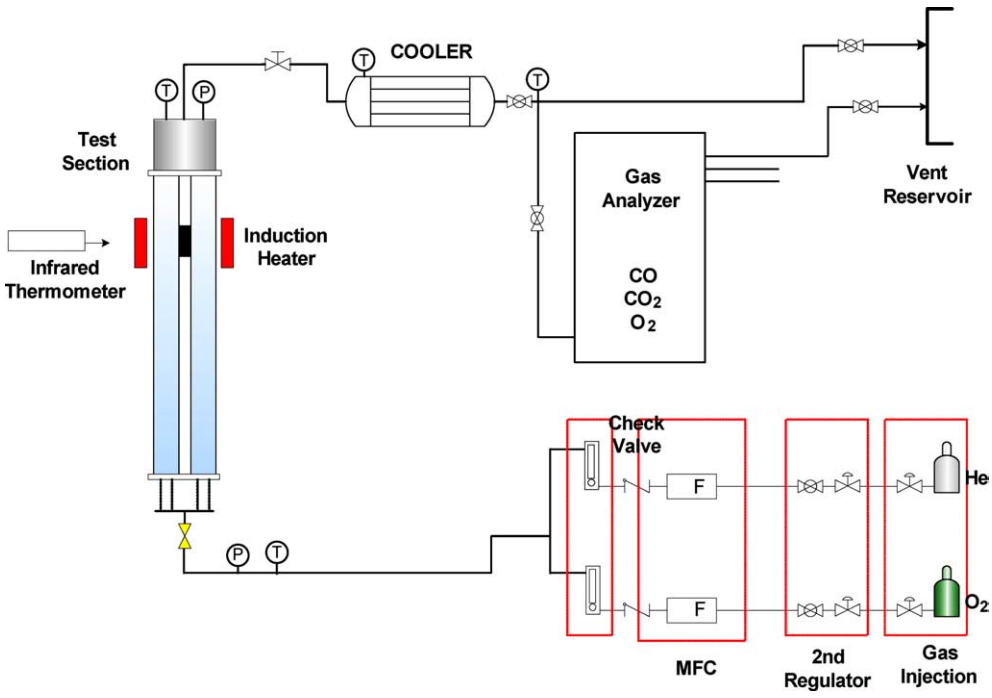

Fig. 1. Schematic diagram of experimental facility.

Table 1
Properties of IG-110 graphite

Material	IG-110
Producer	Toyo Tanso
Bulk density (g/cm^3)	1.75
Young modulus (GPa)	9.6
Compressive strength (MPa)	70.5
Rockwell hardness (MPa)	74.2
Fracture toughness (MPa)	0.82
Thermal conductivity (W/mK)	116
Porosity (vol.%)	21.6
Impurities (ppm)	<20

Table 2
Experimental conditions

	Pretest	Main test
Temperature (°C)	540–600	700–1500
Flow rate (SLPM)	3–18 SLPM (0.072 m/s)	40 SLPM (0.16 m/s)
Inlet oxygen fraction (%)	2.5–32%	2.5%, 5%, 10%, 20%

As a test material, isotropic fine-grained IG-110 graphite was selected in this study. Its properties are summarized in Table 1. Temperature, oxygen concentration, and flow rate were selected as the main experimental variables and the conditions are summarized in Table 2.

2.2. Experimental procedure and data analysis

The following procedure was used:

(1) He gas is injected into the test section at the set flow rate.
(2) When the oxygen concentration in the test section reaches 0%, the graphite specimen is heated to the set temperature.
(3) When the temperature is stabilized, oxygen gas flow is injected into the test section mixed with He gas.
(4) The emitted gas is continuously sampled into the gas analyzer and the concentration data is accumulated.
(5) The reaction rate and CO/CO_2 ratio are calculated from the measured data.

The reaction rate was calculated using the following equation:

$$R_g\ (\mathrm{kg/s}) = M_{w,C} \cdot \frac{\dot{m}_{O_2}}{(X_{O_2} + X_{CO_2} + 1/2X_{CO})} \cdot (X_{CO_2} + X_{CO}), \quad (4)$$

where $M_{w,C}$ is the molecular mass of carbon and $\dot{m}_{O_2}$ is the mass flow rate of oxygen gas. X_i is the mole fraction of the species i in the reacted gases. This equation was derived from the conservation law of total oxygen species between the inlet and outlet gas flow.

3. Results and discussion

3.1. Measurement of oxidation parameters

It is well known that the graphite oxidation rate follows an Arrhenius-type equation:

$$R_g\ (\mathrm{kg/s}) = K_0 \cdot e^{-\frac{E_a}{RT}} \cdot p_{O_2}^n \cdot A. \quad (5)$$

We determined E_a and n in the pretest as described in Section 2.2. We subsequently utilized these pretest results as the input data for code calculation (see Section 3.3).

3.1.1. Activation energy (E_a)

Fig. 2(a) shows an example of the results measured at 5.05% oxygen mole fraction. Our result shows good agreement with Arrhenius-type model. We have performed a total of 33 tests at various conditions, and we illustrated them in Fig. 2(b). Each symbol denotes a different flow rates. This figure shows that the activation energy E_a is not sensitive to flow rate and it confirms that the chemical effects are only rate-determining process in our experimental conditions. Our results can be summarized as follows:

(a) $E_a = 218 \pm 4$ kJ/mol within a 95% level of confidence.
(b) E_a is not affected by oxygen concentration, as Hinsen et al. [2] showed.

Table 3 summarizes the previous and our activation energies measured for the same graphite material. This table shows that the activation energies of Fuller and Okoh [3], Ogawa [4] and Kawakami [5] are very close to ours and it confirms that 200–220 kJ/mol is a reasonable value for the activation energy of IG-110 graphite.

3.1.2. Order of reaction (n)

To obtain the order of reaction, we measured the reaction rate at different oxygen concentrations and illustrate them in Fig. 3(a).

This graph shows that the n values ranged from 0.6 to 0.9. To increase the statistical reliability, we

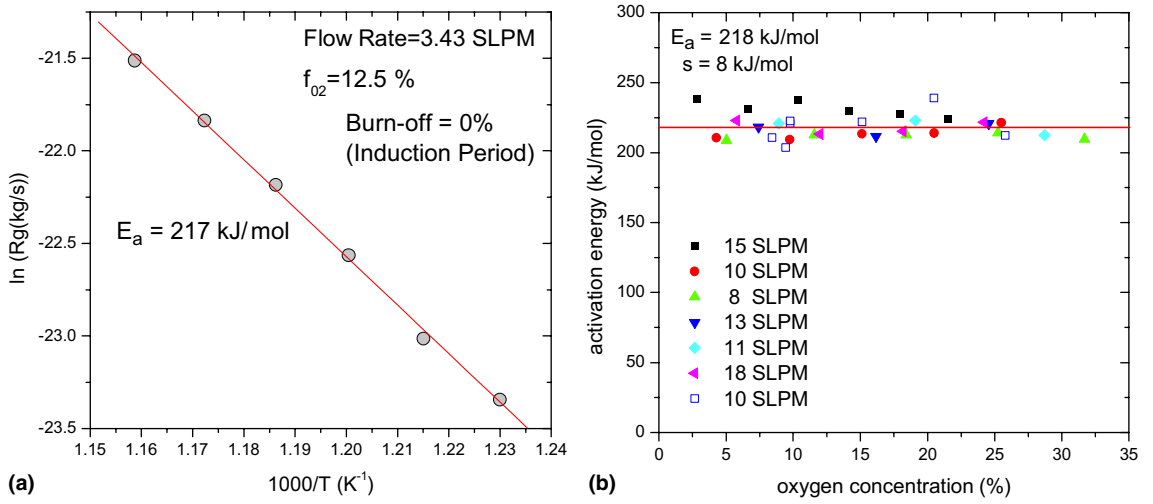

Fig. 2. (a) Arrhenius plot. (b) Summary of activation energy results for different flow rates and oxygen concentrations at 540–600 °C.

Table 3
Summary of previous experimental results for IG-110

Author (material)	T (°C)	Oxygen mole fraction	Flow rate (SLPM)	E_a (kJ/mol)	n	Method
Fuller and Okoh [3]	450–750	0.2	0.496	201	–	TGA
Kawakami [5]	550–650	0.2	–	210	0.76–1.06	Gas analysis
Ogawa [4]	700–1500	0.05–0.19	0.2–4.5	200	–	Gas analysis
KAIST (present study)	540–630	0.03–0.32	7–18	218	0.75 ± 0.15	Gas analysis

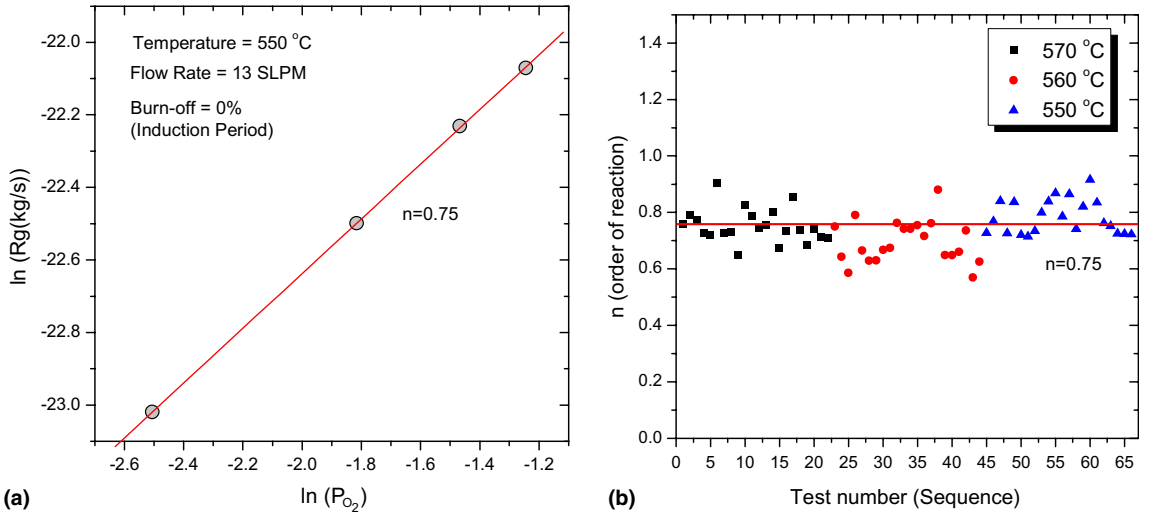

Fig. 3. (a) Effect of oxygen pressure on oxidation rate. (b) Summary of results for the order of reaction at different temperatures.

conducted tests at several conditions and obtained 66 sets of data. Fig. 3(b) illustrates the results. As shown in Fig. 3(b), the distribution of n value does not show any trend with temperature, sample or flow rate. So we analyzed the data by general descriptive statistics. As a result, 0.75 ± 0.146 was obtained within 95% level of confidence.

3.2. Main test results

The main test was performed at similar conditions to an air-ingress accident of a HTGR. In this test, we measured the reaction rate and relative fractions of CO and CO_2. It has been reported by the previous researches that the rate of reaction varies

with the degree of burn-off and the detail mechanism was well explained by Fuller and Okoh [3]: after a slow start and an induction period, the rates accelerate as more porosity created and then decline after passing through a maximum. However, since the main focus of this study is on the combined effect of kinetics and mass diffusion in the wide ranges of temperature and oxygen pressure, the effect of burn-off is not considered in this paper. Therefore, all the data included here represent only induction period where the degree of burn-off is nearly zero. In the induction period, all the specimens have the same original characteristics. The data of Fig. 4 represent the initial oxidation rates during the test. The reaction rate becomes saturated at higher temperatures, where mass transfer becomes rate-determining step.

Fig. 5 shows the experimental results for the CO/CO_2 ratio. In this graph, our data and those of Takahashi et al. [6] are included. The latter experiment [6] was performed with the same graphite material as ours.

The CO/CO_2 ratio data was compared with the previous Aurthur's and Rossberg's correlations.

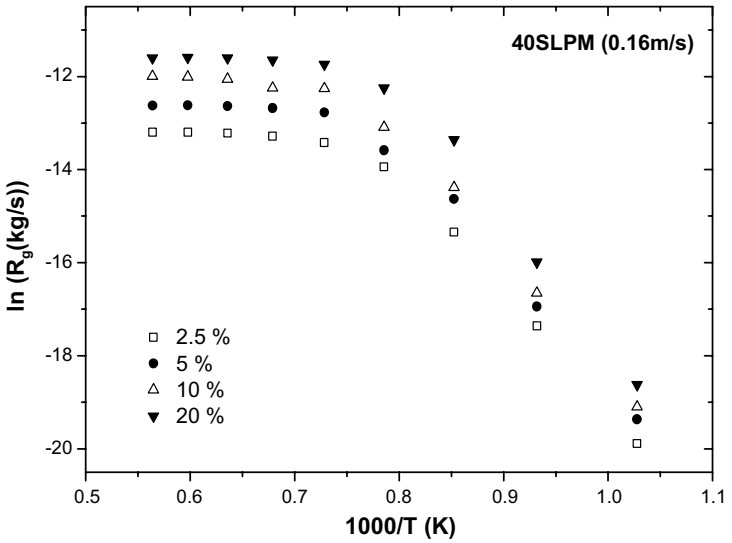

Fig. 4. Arrhenius plot for the main test at different O_2 concentrations.

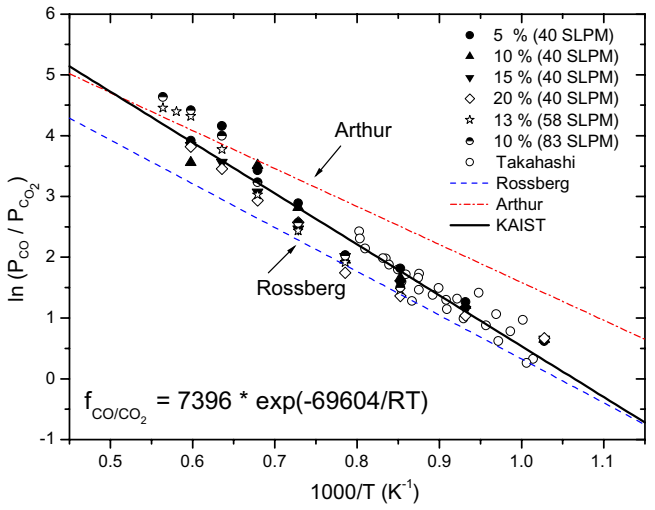

Fig. 5. CO/CO_2 ratio.

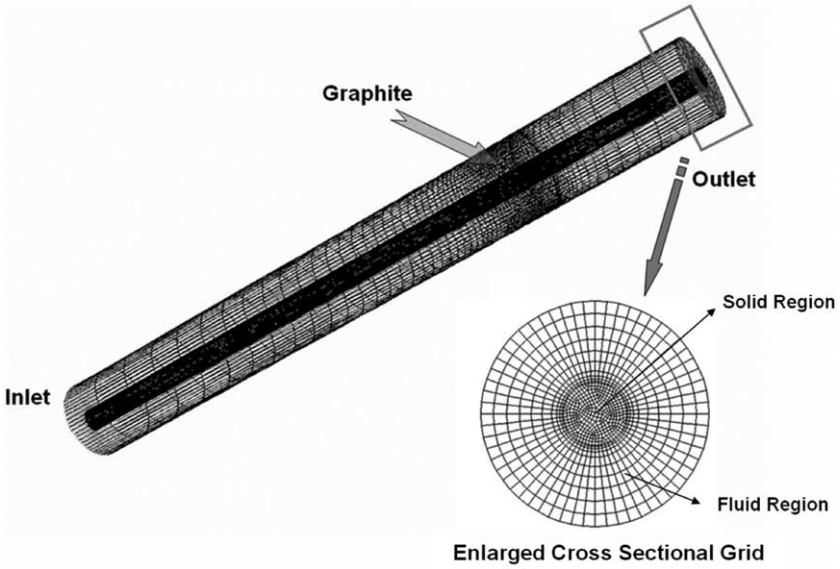

Fig. 6. CFD simulation grid.

Aurthur [7]:

$$f_{CO/CO_2} = 10^{3.4} \exp\left(-\frac{51\,900}{RT}\right).$$

Rossberg [8]:

$$f_{CO/CO_2} = 10^{3.27} \exp\left(-\frac{59\,900}{RT}\right).$$

Rossberg [8] obtained the product ratio for the oxidation of two electrode carbons in the temperature range of 520–1420 °C. Aurthur [7] derived the above expression for coal char and natural graphite. As shown in Fig. 5, the data was distributed between Aurthur's and Rossberg's correlations. The 30% overprediction for Aurthur's and The 20% underprediction for Rossberg's were observed here. Especially the latter shows quiet good agreements with our experimental data even though different material may be expected to have different CO/CO_2 ratios. Most of data lie between their predictions. Here, for the better prediction for IG-110, an empirical correlation was suggested

$$f_{CO/CO_2} = 7396 \exp\left(-\frac{69\,604}{RT}\right). \quad (6)$$

3.3. CFD simulation

We used a CFD simulation to calculate a theoretical reaction rate. This approach was selected for the following reason. In an air-ingress accident, the temperature of the reactor core increases to nearly 1600 °C. In this situation, the graphite oxidation reaction is largely affected not only by reaction chemistry but also by mass transfer by local distribution of flow, temperature, pressure, and gas components. The CFD simulation allows one to estimate the distribution of local parameters without any further assumption regarding wall friction or heat transfer, as long as the chemical kinetic parameters and the CO/CO_2 ratio are well defined.

Fig. 6 shows the grid of this simulation. Fluent 6.1 software was selected as the CFD tool to simulate the main test. The geometry was hexagonally meshed to 77274 nodes. We used the oxidation parameters ($E_a = 218$ kJ/mol, $n = 0.75$) developed here and the CO/CO_2 ratio correlation (Eq. (6)).

The governing equations used in Fluent for our simulation is summarized in Table 4. Total of 8 transport equations were solved here for each node: 1 mass conservation, 3 momentum conservation, 1 energy conservation, and 3 species conservation equations. Since the experimental conditions are in the laminar flow regime, turbulent effects were neglected. Inlet velocity and outlet pressure were given as boundary conditions. During the simulation, the constant wall temperature condition was imposed at the graphite wall. Fig. 6 shows the cross-sectional grid scheme. In this figure, the center region is a solid part and the outer region is a fluid

Table 4
Governing equations for CFD simulation

1. Mass conservation

$$\frac{\partial \rho}{\partial t} + \nabla \cdot (\rho \vec{v}) = S_{\mathrm{m}}.$$

2. Momentum conservation

$$\frac{\partial}{\partial t}(\rho \vec{v}) + \nabla \cdot (\rho \vec{v}\vec{v}) = -\nabla p + \nabla \cdot (\bar{\tau}) + \rho \vec{g} + \vec{F},$$
$$\bar{\tau} = \mu \left[\nabla \vec{v} - \frac{2}{3} \nabla \cdot \vec{v} I \right].$$

3. Energy conservation

$$\frac{\partial}{\partial t}(\rho E) + \nabla \cdot (\vec{v}(\rho E + p)) = \nabla \cdot \left(k_{\mathrm{cond}} \nabla T - \sum_j h_j \vec{J}_j \right) + S_{\mathrm{heat}},$$
$$E = h - \frac{p}{\rho} + \frac{v^2}{2} \quad \left(h = \sum_j Y_j h_j \right).$$

4. Species conservation

$$\frac{\partial}{\partial t}(\rho Y_i) + \nabla \cdot (\rho \vec{v} Y_i) = \nabla \cdot \vec{J}_j + r_i'''.$$
$$\vec{J}_j = -\sum_{j=1}^{N-1} \rho D_{ij} \nabla Y_j \text{ (full multicomponent diffusion model)},$$
$$r'''_{\mathrm{O_2}} = -\frac{M_{\mathrm{w,O_2}}}{M_{\mathrm{w,C}}} \cdot r_{\mathrm{g}} \cdot \frac{f_{\mathrm{CO/CO_2}} + 2}{2 f_{\mathrm{CO/CO_2}} + 2},$$
$$r'''_{\mathrm{CO}} = \frac{M_{\mathrm{w,CO}}}{M_{\mathrm{w,C}}} \cdot r_{\mathrm{g}} \cdot \frac{f_{\mathrm{CO/CO_2}}}{f_{\mathrm{CO/CO_2}} + 1},$$
$$r'''_{\mathrm{CO_2}} = \frac{M_{\mathrm{w,CO_2}}}{M_{\mathrm{w,C}}} \cdot r_{\mathrm{g}} \cdot \frac{1}{f_{\mathrm{CO/CO_2}} + 1}.$$

part. To reduce the numerical error, the fluid part was symmetrically meshed. In the fluid region, all transport equations were solved while in the solid region, only energy equation was.

Table 5 summarizes the equations for the gas properties which we used here. Density was calculated by ideal gas law, and viscosity was calculated by general multicomponent model. The thermal conductivity and heat capacity for each species were calculated by polynomial functions and mass averaged values were used for mixture values. Species diffusion was calculated by full multicomponent diffusion model, so a single value of mixture diffusion coefficient was not calculated here. The example of calculated gas properties were illustrated in Fig. 7.

Fig. 8 shows a comparison of reaction rate between the simulation and experiment. Good agreement was observed in the comparison. The CFD simulation showed quantitatively good agreement, but it can also give us the following qualitatively important information.

Fig. 9 shows the velocity field around the reacting graphite material. There is a large distortion of the field around the surface by the large amount of

Table 5
Physical equations for material properties of CFD simulation

1. Density

$$\rho = \frac{p}{RT\sum_i \frac{Y_i}{M_{w,i}}} \text{ (ideal gas law)}.$$

2. Viscosity

$$\mu = \sum_i \frac{X_i \mu_i}{\sum_j X_i \Phi_{ij}} \text{ (multicomponent model)},$$

$$\phi_{ij} = \frac{\left[1 + \left(\frac{\mu_i}{\mu_j}\right)^{1/2}\left(\frac{M_{w,j}}{M_{w,i}}\right)^{1/4}\right]^2}{\left[8\left(1 + \frac{M_{w,i}}{M_{w,j}}\right)\right]^{1/2}}.$$

3. Heat capacity

$$C_p = \sum_i Y_i C_{P_i} \text{ (mass fraction average of the pure species heat capacities)}.$$

4. Conductivity

$$k_{cond} = \sum_i Y_i k_{cond,i} \text{ (mass fraction average of the pure species conductivities)}.$$

5. Diffusion coefficient

$$\vec{J}_j = -\sum_{j=1}^{N-1} \rho D_{ij} \nabla Y_j,$$

$$D_{ij} = [D] = [A]^{-1}[B],$$

$$A_{ii} = -\left(\frac{X_i}{D_{iN}}\frac{M_w}{M_{w,N}} + \sum_{\substack{j=1 \\ j\neq i}}^{N} \frac{X_i}{D_{ij}}\frac{M_w}{M_{w,i}}\right), \quad A_{ij} = -X_i\left(\frac{1}{D_{ij}}\frac{M_w}{M_{w,j}} + \frac{1}{D_{iN}}\frac{M_w}{M_{w,N}}\right),$$

$$B_{ii} = -\left(X_i\frac{M_w}{M_{w,N}} + (1 - X_i)\frac{M_w}{M_{w,i}}\right), \quad B_{ij} = -X_i\left(\frac{M_w}{M_{w,j}} - \frac{M_w}{M_{w,N}}\right).$$

gas produced on the graphite wall. Fig. 10 shows the gas concentration pattern around the graphite surface. Note that the CO concentration near the surface is much higher than in the bulk flow.

3.4. Modeling and assessment

A CFD simulation shows very good performance, but it always requires a large amount of computation time and big memory size due to a large number of grids. In actual applications such as nuclear system analysis or safety analysis, generating fine meshes for the whole complicated system is unrealistic due to its limited memory size and computation time. For this reason, system analysis codes which use course grids are more generally used. As the course grid does not calculate detail distributions for temperatures, velocities or properties as done in

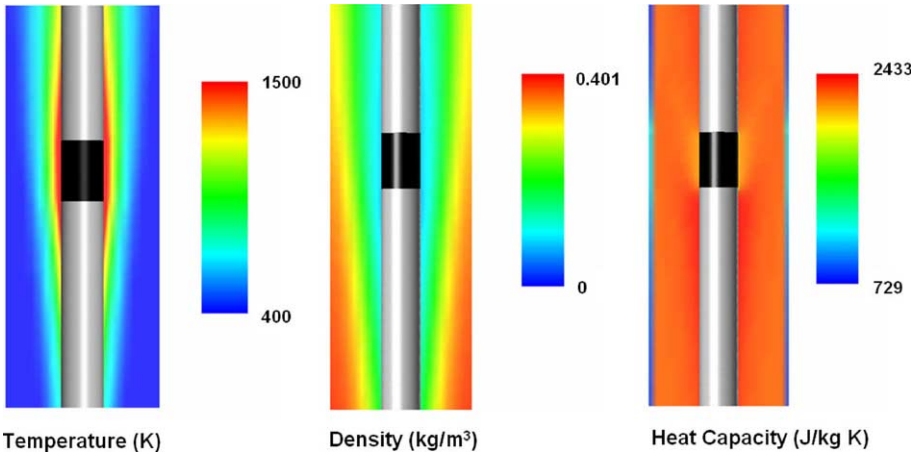

Fig. 7. Calculated temperature and gas properties (1500 °C, 0.16 m/s, 20% of O_2).

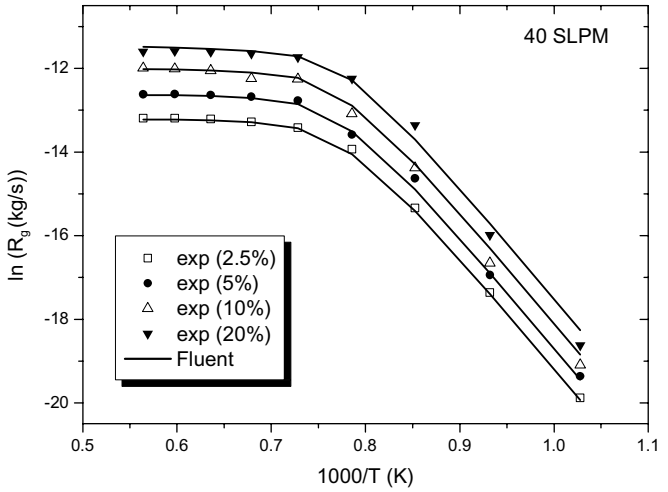

Fig. 8. Comparisons of CFD simulation with experimental results.

the CFD simulation, a lot of constitutive models and correction methods are frequently required.

In this study, a semi-empirical constitutive model, which is applicable for the wide ranges of graphite oxidation, was developed from the following balance equation:

$$k \cdot C_{s,O_2}^{n} = K_m \cdot (C_{b,O_2} - C_{s,O_2}), \tag{7}$$

where the left and right terms mean chemical reaction rate and external mass transfer rate. Since Eq. (7) is an analytically unsolvable equation besides $n = 1$ or 2, numerical method should be used for a general n. However, to avoid numerical calculations, a semi-empirical solution was developed by the following slight modification of the well known solution for $n = 1$. The solution of $n = 1$ can be easily derived as follows [9]:

$$r_g = k \cdot C_{s,O_2}, \tag{8}$$

$$m'' \ (\mathrm{kg/m^2 s}) = K_m \cdot (C_{b,O_2} - C_{s,O_2}). \tag{9}$$

Balancing the above two equations, that is, $r_g = m''$, yields C_{s,O_2}

$$C_{s,O_2} = C_{b,O_2} \cdot \frac{K_m}{K_m + k}. \tag{10}$$

Note that, as the temperature approaches zero, C_{s,O_2} approaches C_{b,O_2}. And as the temperature approaches an infinite value, C_{s,O_2} approaches 0 as expected. Then, the chemical reaction flux becomes

$$r_g = \frac{(K_m \cdot C_{b,O_2}) \cdot k}{K_m + k}. \tag{11}$$

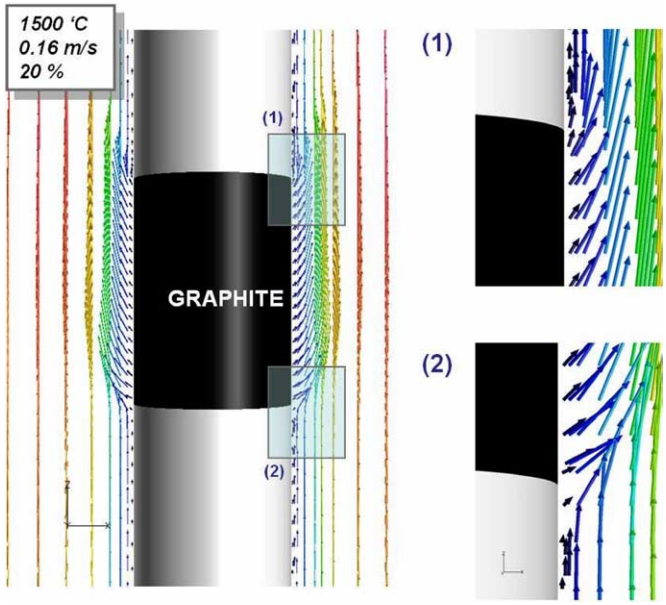

Fig. 9. Simulation results of velocity vectors around graphite material.

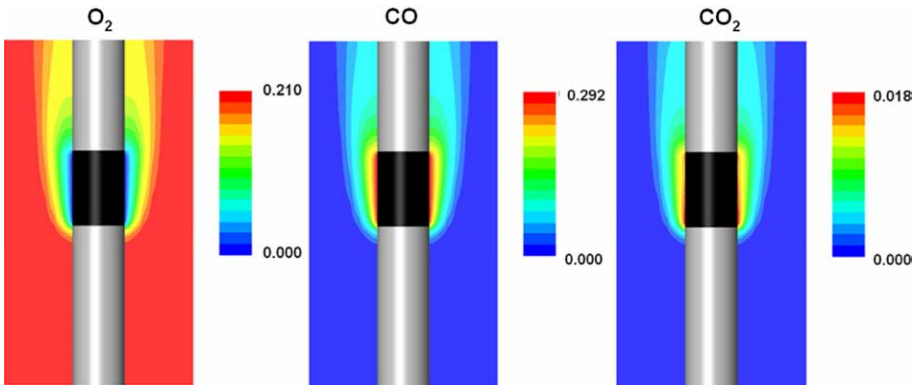

Fig. 10. Simulation results of gas concentrations (1500 °C, 0.16 m/s, 20% of O_2).

This is the general form of the solution for $n = 1$. This equation can be rearranged as follows:

$$r_g = \frac{(K_m \cdot C_{b,O_2}) \cdot (k \cdot C_{b,O_2})}{(K_m \cdot C_{b,O_2}) + (k \cdot C_{b,O_2})}. \tag{12}$$

Then, it is changed into the following:

$$\frac{1}{r_g} = \frac{1}{r_{mb}} + \frac{1}{r_{cb}}, \tag{13}$$

where r_g is an overall reaction rate, r_{mb} is an asymptotic mass transfer flux and r_{cb} is an asymptotic chemical reaction flux. In this solution, all terms are separated by independent simple flux terms. The physical meaning of this solution is that the overall reaction rate approaches r_{cb} as the chemical reaction becomes slower, and conversely, it approaches r_{mb} as the chemical reaction becomes faster. Then, we can assume that replacing the above chemical reaction term, r_{cb} with the following general form (Eq. (16)) will not change its original physical meaning:

$$\frac{1}{R_g} = \frac{1}{R_{mb}} + \frac{1}{R_{cb}}, \tag{14}$$

where

$$R_{mb} = K_m \cdot C_{b,O_2} \cdot A, \tag{15}$$

$$R_{cb} = K_0 \cdot e^{-\frac{E_a}{RT}} \cdot P^n_{O_2,b} \cdot A \quad (n \neq 0). \tag{16}$$

This semi-empirical model becomes exactly the same equation as the original one, Eq. (11), for $n = 1$.

We compared the calculated results with the experimental data for assessment of this correlation. To calculate the mass transfer coefficient, k_m, we used heat/mass transfer analogy [10] and the following Graetz solution [11], which includes the effect of the entrance effect

$$Sh = \frac{k_m \cdot d}{D} = 3.66 + \frac{0.0668(d/x) \cdot (Re \cdot Sc)}{1 + 0.04 \cdot [(d/x) \cdot (Re \cdot Sc)]^{2/3}}. \quad (17)$$

In the reaction entrance region, since the diffusion boundary layer is not fully developed, the boundary layer thickness is much smaller than the fully developed flow. Since the boundary layer thickness is inversely proportional to the mass transfer rate, the mass transfer rate will be underestimated by the normal correlations assuming the fully developed flow. In fully developed region, the Graetz solution shows the same results as the normal correlations.

Generally, most of the mass transfer coefficient correlations are derived by well-known velocity fields, which are assumed for no mass transfer. This is a good assumption for low reaction rate condition. However, it is not suitable for high reaction rate, because such high mass transfer will cause the large velocity distortion. Therefore, for more accurate calculations, a correction is required. In this study, the following correction was performed [12]:

$$k_m^{\text{corrected}} = \theta \cdot k_m, \quad (18)$$

where

$$\theta = \frac{\ln(B_m + 1)}{B_m}, \quad (19)$$

$$B_m = \frac{X_{O_2,b} - X_{O_2,0}}{X_{O_2,b} - 1}. \quad (20)$$

To calculate the mass transfer coefficient from Eq. (17), diffusion coefficient should be decided. A binary diffusion coefficient is generally the most frequent selection. But at high reaction rate, it is not suitable because the gases produced at the reacting surface will affect the gas properties, especially diffusion coefficients. For an exact calculation, multicomponent diffusion model should be used as in the CFD simulation. But because of its complexity, the following effective diffusion coefficient, which means an averaged diffusion coefficient for gas mixture was used here [13].

$$D_{O_2,m} = \frac{(1 - X_1)}{\sum_{i=2}^{n}(X_i / D_{O_2,i})}. \quad (21)$$

Fig. 11 illustrates the comparisons on the oxidation rate between Eq. (14) and experimental data. As shown in this figure, the calculated results are in good agreement with the experimental data within 10% for the whole temperature ranges. It means the Eq. (14) is a useful model for predicting the oxidation rate including combined effect of kinetics and mass diffusion. In this study, though

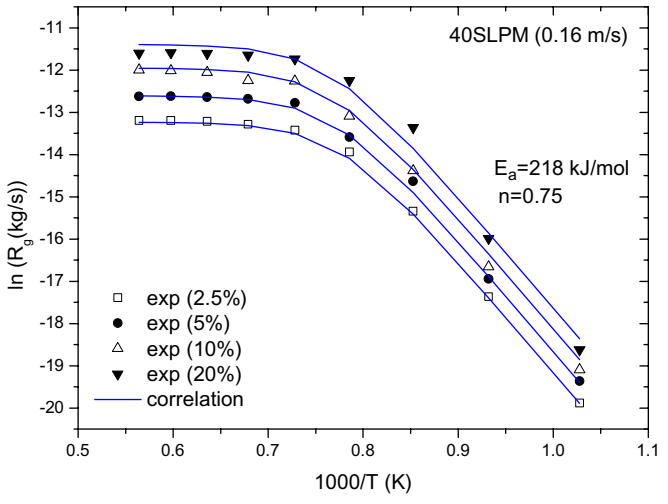

Fig. 11. Comparison results between correlation and experiment.

Eq. (14) was only confirmed in the induction period, we can easily expand this equation to the higher burn-off level, because the model was derived for general cases and each effect (kinetics and mass diffusion) in Eq. (14) is separated as independent terms not to be related to each other.

4. Conclusions

The order of reaction (n) was estimated as 0.75 ± 0.146 with a 95% confidence level. It is insensitive to the burn-off level and oxidation temperature. The activation energy (E_a) was obtained for different oxygen concentrations and flow rates, 218 ± 3.76 kJ/mol was not affected by oxygen concentration.

A graphite oxidation model is proposed to cover the entire temperature range of interest for high temperature gas-cooled nuclear reactors, and was validated against the data. Models for mass transfer correction and entrance consideration are suggested for better prediction of graphite oxidation.

References

[1] P.L. Walker, F. Rusinko, L.G. Austin, Adv. Catal. 11 (1958) 133.
[2] H.K. Hinsen, W. Katscher, R. Moorman, Kinetics of the graphite/oxygen reaction in the in-pore diffusion controlled regime, KFA, 1983, ISSN0366-0885.
[3] E.L. Fuller, M.J. Okoh, J. Nucl. Mater. 240 (1997) 241.
[4] M. Ogawa, Jpn. Nucl. Soc. 35 (3) (1993) 245.
[5] H. Kawakami, TANSO 124 (1986) 26.
[6] M. Takahashi, M. Kotaka, H. Sekimoto, J. Nucl. Sci. Technol. 31 (12) (1994) 1275.
[7] J. Aurthur, Trans. Faraday Soc. 47 (1951) 164.
[8] M.Z. Rossberg, Elektrochemistry 60 (1956) 952.
[9] A.F. Mills, Mass Transfer, Prentice-Hall, Upper Saddle River, NJ, 2001, p. 47.
[10] J.R. Welty, C.E. Wicks, R.E. Wilson, Fundamentals of Momentum, Heat and Mass Transfer, John Willey, 1969, p. 606.
[11] S. Kakac, Y. Yener, Convective Heat Transfer, CRC Press, 1994, p. 147.
[12] A.F. Mills, Mass Transfer, Prentice-Hall, Upper Saddle River, NJ, 2001, p. 153.
[13] A.F. Mills, Mass Transfer, Prentice Hall, Upper Saddle River NJ, 2001, p. 29, 87.